Slope stability analysis application of a static discrete element method

Application d'une méthode statique d'éléments discrets pour l'analyse de la stabilité de pentes

C. L. Ho – *University of Massachusetts, Amherst, Mass., USA*
A. Rodríguez-Marek – *University of California, Berkeley, Calif., USA*
B. Muhunthan – *Washington State University, USA*

SYNOPSIS: This paper presents a static discrete elements method for stability analysis of slopes. The slope is discretized into a series of blocks and the equilibrium of the individual blocs as well as the displacement compatibility between blocks are satisfied. The usual assumptions on interslice force distribution and constant factor of safety made in traditional methods of slices are not used. The method is also not constrained by the evaluation of stability along a predetermined critical surface. The failure surface is determined from the displacement field for the slope. However, a factor of safety can be obtained if the method is applied to a predetermined failure surface. The method is evaluated in the analysis of two slides in overconsolidated clay in which progressive failure was a large factor.

1 INTRODUCTION

The assessment of the stability of natural and man-made earth slopes constitutes one of the most frequent problems encountered by geotechnical engineers. Safety may be assured by providing for qualitative aspects of the design (choice of materials, drainage, geometry, timing of construction), and by the use of an appropriate method of analysis. All but a few of the methods which have traditionally been used to analyze slope stability are based on the principle of limit equilibrium i.e., equilibrium conditions at the point of incipient failure. The strength of limit equilibrium methods (LEMs) is their simplicity. The value of a global safety factor based on the limit state is used to determine whether a slope is stable or not. These methods, however, are developed within a restricted framework: i) slip surfaces must be predetermined, and ii) effects of initial state of stress and stress/strain history, soil stress-strain relations, stress/strain paths to failure, and differing constraints on boundary displacements are not considered in modeling the potential range in distribution of interslice forces.

Apart from a safety factor it is often desirable to have some information about the development of failure (should it occur). Instrumentation can then be suitably placed to give prior warning of the onset of a dangerous situation. LEMs are not capable of the determination of failure initiation and likely collapse mechanism. The finite element method (FEM) is useful to examine the effects of the above factors, and is also capable of showing the initiation of failure.

Recent research efforts have focused on describing the behavior of a soil mass using discrete elements (e.g. Cundall 1971; Walton 1992). This paper presents a discrete block method for the computation of slope stability. The slope is discretized into a number of discrete blocks rather than slices. The usual assumptions on interslice force distributions and a constant factor of safety used in LEMs are replaced with equations of equilibrium and compatibility for individual blocks. The solution algorithm uses the static equilibrium of the discretized blocks rather than the dynamic one used by most current discrete element models. The technique is an extension of a previous study by Chang (1992) and includes a more realistic representation of the soil interface behavior. The failure surface results from the analysis in the new technique. It need not be input at the beginning of the analysis as in Chang (1992). The method is capable of taking into account important factors relating to the progressive nature of slope failures.

The formulation of the proposed technique is summarized herein. The technique is illustrated for two case studies and the results are compared with analysis in the literature. The capability of the method to model progressive failure of slopes is highlighted.

2 INTERFACE BEHAVIOR

A detailed description of the technique is presented elsewhere (Rodríguez-Marek 1996, Rodríguez-Marek et al. 1996), and a summary is presented herein. The slope is discretized into a series of blocks joined together by Winkler springs. The Winkler springs simulate the load-deformation behavior of the soil. The springs have normal and shear stiffness given by k_n and k_s respectively. The normal and shear springs have elasto-plastic characteristics. The normal springs do not yield in compression, but they do in tension, beyond the tensile capacity of the soil. The "tension cutoff" is provided for cohesive soils but not for cohesionless soils. After reaching the tension cut-off, the normal soil resistance is assumed to drop immediately to zero (Figure 1a). The shear springs yield when the shear strength is reached. For plastic soils, the peak strength is governed by the Mohr-Coulomb criterion:

$$\tau_p = c'_p + \sigma'_n \tan\phi'_p \qquad (2.1)$$

where τ_p is the peak strength, c'_p is the effective peak cohesion, σ_n is the effective normal stress, and ϕ'_p is the effective peak friction angle. Beyond the peak strength, the strength parameters c'_p and ϕ'_p of plastic strain softening soils are reduced to their residual values c'_r and ϕ'_r respectively, in Equation 2.1. The interface shear behavior of the soil is shown in Figure 1b. Notice that the residual strength is achieved at large deformations.

3 MECHANICS OF DISCRETE BLOCKS

The equilibrium and compatibility equations are derived for two interactive blocks A and B (Figure 2). Let P be the midpoint of the interface between these two blocks. Let $\underline{r}^{ip}$ be a vector pointing from the centroid of block i to the point P. Let $\underline{u}^a$ and $\underline{u}^b$ be vectors representing centroid displacements of blocks A and B. These vectors include the block displacements in global x and y directions (u_x and u_y), and the block rotation (u_ω). The

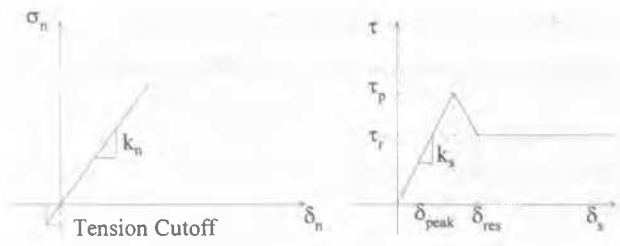

a) normal Winkler spring b) shear Winkler spring

Figure 1. Behavior of normal and shear Winkler springs (stress vs. Displacement). (From Rodríguez-Marek et al. 1996).

displacement of block B relative to block A, at point P, $\underline{\Delta}^P$, is (Chang 1992):

$$\begin{Bmatrix} \Delta_x^P \\ \Delta_y^P \\ \Delta_\omega^P \end{Bmatrix} = \begin{bmatrix} 1 & 0 & -r_y^{bp} \\ 0 & 1 & r_x^{bp} \\ 0 & 0 & 1 \end{bmatrix} \begin{Bmatrix} u_x^b \\ u_y^b \\ u_\omega^b \end{Bmatrix} - \begin{bmatrix} 1 & 0 & -r_y^{ap} \\ 0 & 1 & r_x^{ap} \\ 0 & 0 & 1 \end{bmatrix} \begin{Bmatrix} u_x^a \\ u_y^a \\ u_\omega^a \end{Bmatrix} \quad (3.1)$$

The relative movements of the two interacting blocks at any point P' on the interface result in spring displacements in the normal direction, δ_n, and in the shear direction, δ_s, given by:

$$\delta_n = \Delta_n^P + \Delta_\omega^P \, l \quad (3.2a)$$

$$\delta_s = \Delta_s^P \quad (3.2b)$$

where l is the distance from the center point P to point P', and displacements Δ^P are expressed in a local coordinate system, where subscripts n and s indicate normal and shear movement, respectively, and subscript ω indicates rotation.

The spring displacements, in turn, generate normal and shear stresses on the block interface as shown in Figure 2. Integration of these stresses over the interface length result in the following relationships between the resultant forces and moments at point P and the displacements and rotations at the same point (Chang 1992, Rodríguez-Marek 1996):

$$\begin{Bmatrix} F_n^P \\ F_s^P \\ M^P \end{Bmatrix} = \begin{bmatrix} K_n & 0 & 0 \\ 0 & K_s & 0 \\ 0 & 0 & K_\omega \end{bmatrix} \begin{Bmatrix} \Delta_n^P \\ \Delta_s^P \\ \Delta_\omega^P \end{Bmatrix} \quad (3.3a)$$

or

$$\{\underline{F}\} = \left[\underline{\underline{K}}_{local}\right]\{\underline{\Delta}^P\} \quad (3.3b)$$

where $K_n = k_n L$, $K_s = k_s L$, $K_\omega = (k_n L^3)/12$, $\underline{F}$ is the interface force-moment vector (Figure 2), $\underline{\underline{K}}_{local}$ is the local stiffness matrix, and $\underline{\Delta}^P$ is the displacement vector of point P in local coordinates.

Using coordinate transformations on the local stiffness matrices, and enforcing equilibrium among all the forces acting at the block boundaries, and external forces acting at the centroids of the block, results in the following equation:

$$\{\underline{f}^a\} = \sum_P^N \begin{bmatrix} -1 & 0 & 0 \\ 0 & -1 & 0 \\ r_y^{ap} & -r_x^{ap} & -1 \end{bmatrix} \left[\underline{\underline{K}}\right]\{\underline{\Delta}^P\} \quad (3.4)$$

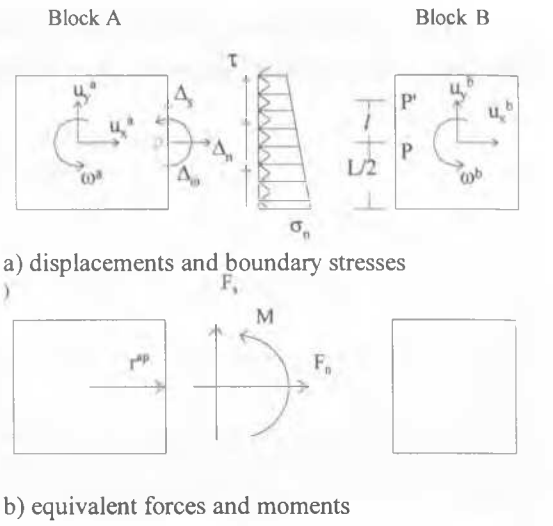

Figure 2. Block displacements, stresses, and equivalent forces. (From Rodríguez-Marek et al. 1996)

where N is the total number of sides of the block, $\underline{f}^a$ is the force-moment vector corresponding to the forces applied at the centroid of block A, and $\underline{\underline{K}}$ is the local stiffness matrix in global coordinates. The above equation gives a relationship between the forces applied at the centroid of block A, and the displacements of the centroids adjacent to block A. The displacements of point P, $\underline{\Delta}^P$, in terms of the displacements of the centroids in the global coordinate system are given by Equation 3.1. Use of Equation 3.4 for each block, and application of displacement compatibility, results in a relationship of the form:

$$\{\underline{f}\} = \left[\underline{\underline{K}}'\right]\{\underline{u}\} \quad (3.5)$$

where $\underline{\underline{K}}'$ is a symmetric banded stiffness matrix relating centroid displacements to the forces applied to the centroid, $\underline{f}$ is the vector of applied forces at the centroid of all blocks, and $\underline{u}$ is the vector of displacements of all blocks. In general cases, the force vector $\underline{f}$ consists only of a vertical gravity load, but may include any other externally applied loads, such as the overburden and seepage forces. The solution of Equation 3.5 is obtained with appropriate displacement boundary conditions.

Once displacements are found, they are used to find forces acting along the block interfaces. The average stress acting on each interface is found by dividing the force over the block length. These stresses are compared with the shear strength of each interface. For boundaries that have yielded, the displacement δ_s (Equation 3.2b) is used to find a new secant stiffness (k_s). The use of a secant stiffness avoids problems originating from the negative modulus during the transition from peak to residual strength (Lo and Lee 1977). Since no interaction is possible in the case of tension cracks, the normal and shear stiffness are switched to zero. The solution algorithm for the method and a discussion on its implementation is presented elsewhere (Rodríguez-Marek 1996, Rodríguez-Marek et al. 1996).

4 CASE STUDIES

4.1 Selset, England

To illustrate the proposed method, a landslide in Selset, England (Skempton and Brown 1961), is analyzed. The slope is 12.8 m high with an inclination of 28°. Peak soil strength parameters are

c'_p = 8.6 kPa, ϕ'_p = 32°. Residual strength parameters are taken as $\phi'_p = \phi'_r$ and $c'_r = 0$. Unit weight of the soil is 21.8 kN/m^3. A pore pressure ratio of 0.45 was used in the analysis. The LEM analysis of the slope using XSTABL (Sharma 1994) with peak strength parameters yielded a minimum factor of safety of 1.02. This value was based on the Morgenstern and Price method (1965). The critical surface was obtained using random surface generation available in XSTABL (Sharma 1994). The failure surface is shown in Figure 3.

The contour plot of the horizontal displacement at the onset of failure, based on the proposed technique, is also shown in Figure 3. The failure surface is observed in this figure as a narrow region of displacement discontinuity. This region is in close agreement with the failure surface obtained in the LEM analysis (Figure 3). A pattern of displacements also appear away from the slope at the right side of the region analyzed. These displacements, however, are two orders of magnitude smaller than the displacements within the failure mass and are negligible. These displacements are artifacts of the numerical method and boundary conditions.

A direct measure of the stability of the slope is sometimes desired. For this purpose, the proposed method is applied to a typical slice geometry using a predetermined failure surface. Local factors of safety are defined by the ratio of available to mobilized strength along the base of each slice. Similarly, a global factor of safety is determined to give a measure of safety for the whole slope. This results in an improved stability analysis without the simplifying assumptions of conventional limit equilibrium (Chang 1992). The propagation of the failure surface can be observed by obtaining local factors of safety along the failure surface in Figure 3 (Figure 4). Localized failure occurs in the crest of the slope and propagates along the failure surface. Furthermore, the analysis reproduced the tension cracks in the crest observed by Skempton and Brown (1961).

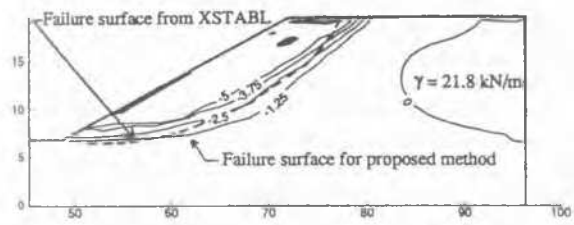

Figure 3. Contour plot of horizontal displacements for Selset slope (from Rodríguez Marek et al. 1996).

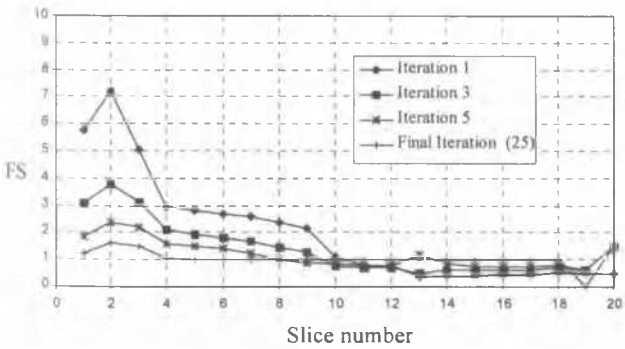

Figure 4. Factors of safety for various iterations. Peak strength parameters. Note that FS = 0 for the final iteration on slice 19. This is an indication of tension cracking (From Rodríguez-Marek 1996).

4.2 Sudbury Hill, England.

The method was also applied to a slope in stiff fissured London Blue Clay in Sudbury Hill, England. Soil parameters and slope geometry are obtained from Law and Lumb (1978). The slope is 7.0 m high with an inclination of 18.4°. The peak soil strength parameters are c'_p = 12.0 kPa, ϕ'_p = 20°. Failure was triggered by regrading of the slope. Initial shear failure on the overconsolidated clay resulted in negative pore pressures. The dissipation of pore pressures caused a reduction of strength leading to a zero effective cohesion. Accordingly, the residual strength parameters are taken as $\phi'_r = \phi'_p$ and $c'_r = 0$. The unit weight of the soil is 18.8 kN/m^3.

The discrete element method analysis resulted in complete failure. The displacement field is shown in Figure 5. The predicted failure surface can be seen as a narrow region of displacement discontinuity. This predicted failure surface matches the observed failure surface (Law and Lumb 1978). A parametric study of the slope showed the failure surface to be sensitive to the location of the level of the water table.

A region of displacement discontinuity is observed below the slope and away from the failure mass. As in the previous example, this is an artifact of the mesh geometry and boundary conditions. Displacements in this region are an order of magnitude smaller than in the failure mass and can be considered negligible.

5 CONCLUSION

This paper presented a static discrete element method for stability analysis of slopes. The slope is discretized into blocks and the solution for their displacements is obtained by solving the equilibrium and displacement compatibility equations. The displacement field of the proposed method can be used to identify the initiation of failure surface. Therefore, the solution is not constrained by the evaluation of stability along a predetermined critical surface, nor by any assumptions regarding force distribution on block boundaries.

The presence of rigid blocks in the analysis model limits lateral stress transfer. This results in lower strength for vertical boundaries (Rodríguez-Marek 1996). This, however, does not seem to affect blocks in the failure regions for relatively shallow slides. Results have also shown a large degree of mesh dependency in the shape of the failure surface.

The method is effective in determining the progressive nature of slope failure in plastic and brittle soils. Furthermore, the application of the method to a slice geometry results in an improved limit equilibrium analysis that accounts for the elasto-

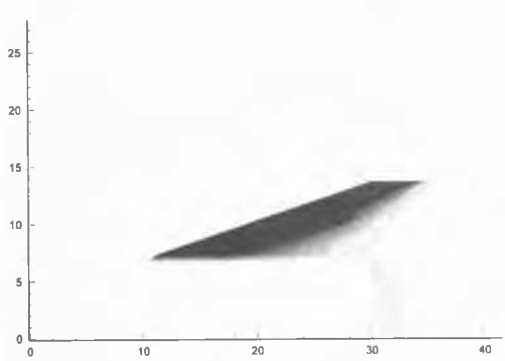

Figure 5. Contour plot of horizontal displacements for Sudbury Hill slope. Darker colors correspond to larger displacements.

plastic behavior of soil. The method is simple and the boundary conditions are easily input without the time constraints associated with finite element methods. The resulting displacement field can be useful in developing design guidelines for stabilizing techniques.

ACKNOWLEDGMENTS

This material is based upon work supported by the National Science Foundation under Grant No. BCS 9222669. Any opinions, findings, and conclusions or recommendations expressed in this material are those of the authors and do not necessarily reflect the views of the National Science Foundation.

REFERENCES

Chang, C.S. 1992. Discrete element method for slope stability analysis. Journal of Geotechnical Engineering, ASCE 118(12): 1889-1903.

Cundall , P.A. 1971. A computer model for simulating progressive, large-scale movements in block rock systems. Proc. Int. Symp. on Rock Fracture, Nancy, France, 1: 8-17.

Law, K.T., and Lumb, P. 1978. A limit equilibrium analysis of progressive failure in the stability of slopes. Canadian Geotechnical Journal, 15(1), 113-122.

Lo, K.Y., and Lee, C.F. 1973. Stress analysis and slope stability in strain softening soils. Geotechnique, 23(1): 1-11.

Morgenstern, N.R., and Price, V.E. 1965. The analysis of the stability of general slip surfaces. Géotechnique, 15(1), 70-93.

Rodríguez-Marek A. 1996. Discrete element method for slope stability analysis. Master's Thesis, Washington State University, Pullman, WA.

Rodríguez-Marek, A., Muhunthan, B. and Ho, C.L. 1996 Discrete Element Method for Slope Stability Analysis. 7th International Symposium on Landslides, Trondheim, Norway.

Sharma, S. 1994. XSTABL, an integrated slope stability analysis program for personal computers. Interactive Software Designs, Inc. Moscow, ID.

Skempton, A.W., and Brown, J.D. 1961. A landslide in Boulder clay at Selset, Yorkshire. Géotechnique, 11(4), 280-293.

Walton, O.R. 1992. Numerical Simulation of inelastic frictional particle-particle interactions. in Particulate two-phase Flow, Roco, M.C. Ed. Butterworth-Heinemann, MA.